Analysis of Dispersion and Series Gap Discontinuity in Shielded Suspended Striplines with Substrate Mounting Grooves

Lin-Kun Wu, *Member, IEEE,* and Horng-Ming Chang

***Abstract*—Dispersion and series gap discontinuity of shielded suspended striplines (SSL's) on Duroid substrate (ε_r = 2.22) are analyzed using the finite-difference time-domain method (FD-TD). Numerical accuracy of better than 0.15% is achieved when the FD-TD is used to calculate the effective dielectric constant (ε_{reff}) of an air-filled rectangular coaxial transmission line. Data obtained for the frequency-dependent ε_{reff} of uniform SSL's, and both scattering and equivalent circuit parameters of various series gap discontinuities, are then presented. In general, presence of sidewall mounting grooves causes a nearly frequency-independent small reduction in ε_{reff}. On the other hand, proximity effects of the housing are found to be more important. It is demonstrated that: 1) for a given housing, ε_{reff} decreases first with an increase in strip width before increasing again when strip is wider enough to interact strongly with the sidewalls and 2) reducing sidewall spacing causes an increase in ε_{reff}. For the gap discontinuity, coupling across the gap is stronger for wider strips and/or narrower gap width. Irregular transmission behavior is also found when strip is wide enough to interact strongly with the sidewalls.**

I. Introduction

SHIELDED suspended striplines (SSL's) have found increasing uses in the design of integrated circuit components in the millimeter-wave region because of their low attenuation, weak dispersion, and small effective dielectric constant [1]–[4]. Although the SSL's can be treated in a unified manner as strip transmission lines containing multiple layers of dielectric materials, a literature search reveals only a relatively limited amount of information on SSL's.

Frequency-dependent dispersion characteristics of uniform SSL's placed in a shielding waveguide have been analyzed in [5]–[7]. Discontinuities including single and parallel-coupled open end(s), and asymmetrical series gap, in a shielded SSL were analyzed in [8] and [9]. In practical use, however, the substrate of the SSL is supported mechanically with grooves in the sidewalls of the shielding waveguide. An analytical model for the calculation of the cutoff frequency of the TE_{10} type of waveguide mode in shielded SSL with mounting grooves is given in [10]. It is shown that the increasing groove depth lowers the TE_{10} cutoff frequency. In [11], the effects of the sidewall grooves on the wavelength reduction factor λ/λ_0 (or the effective dielectric constant ϵ_{reff}) and characteristic impedance Z_0 of SSL's are analyzed within the TEM-wave approximation. It is found that groove effects can be significant for a shallow groove.

In this paper, dispersion and series gap discontinuity in shielded SSL's are characterized by the finite-difference time-domain method (FD-TD) [12]. The method used here evolves from the FD-TD method developed initially for the analysis of open microstrip problems [13], [14] and modified more recently for the analysis of shielded microstrip (with grounded substrate) problems [15]. With the suspension of substrate, a slight change in the spatial distribution of the excitation waveform is needed. In the following, a brief summary of the FD-TD method employed will be given first. Accuracy of the FD-TD is then verified by determining the ϵ_{reff} of an air-filled rectangular coaxial transmission line (RCTL). Numerical results are then presented for various uniform SSL's and SSL's with series gap discontinuity. Effects of mounting grooves are examined along the way.

II. Summary of the Method of Analysis

Consider the cross-section view of the shielded SSL with sidewall mounting grooves shown in Fig. 1. The substrate with thickness h_2 and dielectric constant ϵ_r is suspended at a height of h_1 above the bottom wall of the shielding waveguide. The strip, assumed to be a zero-thickness perfect conductor of width w, is centered between the two sidewalls. The shielding waveguide has a width b and height a, and both mounting grooves have a depth of d and height h_2. For the dispersion properties to be examined, the entire structure extends uniformly into infinities along both $\pm z$ direction. In the case of series gap discontinuity shown in Fig. 2(a), a gap of width g is introduced in the strip pattern. By setting h_1 and d to 0, the SSL shown in Fig. 1 becomes a shielded microstrip [15]. Numerical experiments have confirmed the FD-TD method used in [15] is also applicable to the SSL including sidewall mounting grooves. Therefore, only a brief summary of the FD-TD method is described here.

Manuscript received May 28, 1991; revised September 17, 1991. This work was supported by the National Science Council of the Republic of China under Grant NSC 80-0404-E-009-65.

The authors are with the Institution of Communication Engineering, National Chiao Tung University, 1001 Ta Hsueh Road, Hsinchu, Taiwan 30050, Republic of China.

IEEE Log Number 9104781.

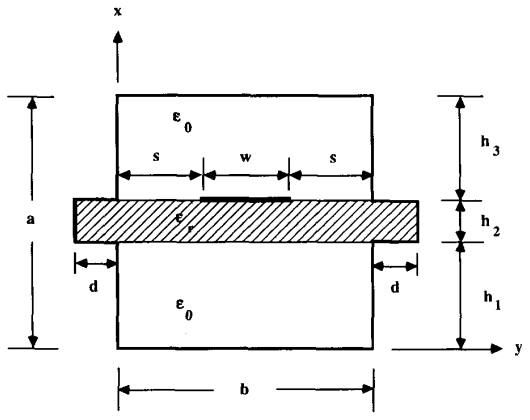

Fig. 1. Cross section of a shielded suspended stripline with sidewall mounting grooves.

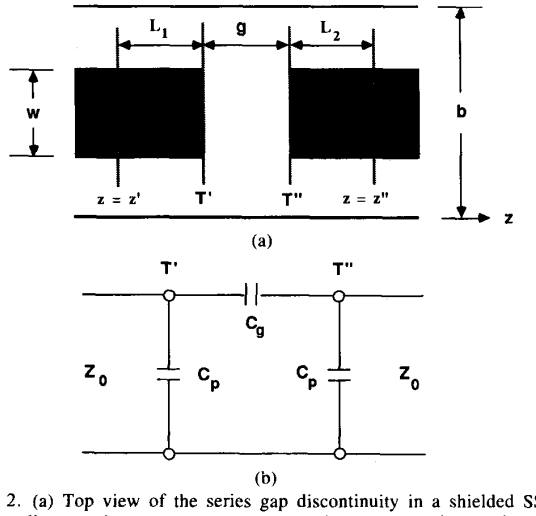

Fig. 2. (a) Top view of the series gap discontinuity in a shielded SSL (sidewall mounting grooves are removed), and (b) its equivalent π-network.

To characterize the dispersion and gap discontinuity of SSL's, propagation of a Gaussian pulse through appropriate SSL structure is simulated using the FD-TD. Following the space and time discretizations of the electric and magnetic field components, the FD-TD equivalents of the Maxwell's curl equations are then used to update the spatial distributions of the electric and magnetic field components at alternating half time steps as time marches on [12], [14]. The spatial cell size, measured (dx, dy, dz) along the x-, y-, and z-direction, is chosen small enough to model the fine structural details and/or field variations. Courant stability criterion [16] is then followed in the selection of the temporal sampling interval to ensure numerical stability.

In contrast to the case of a shielded microstrip with grounded substrate, the source distribution used for the SSL is modified to take into account the discontinuity experienced by the vertical electric field, E_x, when crossing the dielectric-air interface at the plane of excitation (say, $z = 0$). Specifically speaking, in the region between the strip and the bottom waveguide wall, the excitation source is composed of E_x's with the following space-time distribution

$$E_x(x, y; t) = \begin{cases} s(t), & \cdots h_1 \le x \le h_1 + h_2 \\ s(t)/\epsilon_r, & \cdots 0 \le x \le h_1 \end{cases} \quad (1)$$

for $(b - w)/2 \le y \le (b + w)/2$. In (1), $s(t)$ is a Gaussian pulse given by

$$s(t) = \exp\left[-(t - t_0)^2/T^2\right] \quad (2)$$

where T is chosen such that only the dominant (quasi-TEM) mode is propagating in the SSL, and t_0 is selected for smooth turn-on and turn-off of the excitation pulse. It is noted that the value of the signal voltage at a frequency of $f_u = 1/2T$ is only 8.5% that of the peak at dc. Finally, to complete our specifications of the space-time distributions of the excitation, E_x's elsewhere in the plane of $z = 0$ are calculated using the magnetic wall source condition of [17].

The exact boundary conditions are enforced at the perfectly conducting housing walls and the strip conductor, over which only the tangential electric-and/or normal magnetic-field components are sampled and set to zero at all time steps. For the update of tangential electric field components sampled at the two air-dielectric interfaces, average permittivity between the two (i.e., $\epsilon_0(\epsilon_r + 1)/2$ is used in the FD-TD equations. In this way, field continuity condition at the interface is satisfied [14]. Finally, the super-absorbing boundary condition [18] is employed to terminate the FD-TD lattice at the planes of $z = 0$ and $N_z\, dz$(N_z is the number of cells in z-axis).

To determine the frequency-dependent ϵ_{reff}, time waveforms of E_x's sampled at half cell below the center of the strip are recorded at several points along the direction of wave propagation (i.e., z-axis). These waveforms are then fast Fourier transformed to obtain the corresponding pulse spectra, which are denoted as $E_x(z_i, \omega)$ with z_i being the ith sampling point. For frequency below the onset of the first higher-order waveguide mode, the dominant quasi-TEM mode is characterized by a frequency-dependent phase constant $\beta(\omega)$ or effective dielectric constant $\epsilon_{reff}(\omega)$, which can be determined as follows

$$e^{-j\beta(\omega)L} = \frac{E_x(z = z_i + L; \omega)}{E_x(z_i; \omega)} \quad (3)$$

where L is the distance between two arbitrary sampling points and

$$\beta(\omega) = \omega\sqrt{\mu_0\epsilon_0\epsilon_{reff}(\omega)}. \quad (4)$$

Equations (3) and (4) are repeated for each of several possible pairs of $E_x(z_i, \omega)$'s, from which converged data are extracted.

Since the series gap discontinuity shown in Fig. 2(a) is a symmetrical two-port network, only the reflection and transmission coefficients associated with the wave inci-

dent from the left-hand side of the structure, i.e., S_{11} and S_{21}, need be determined. In this case, spectra of the incident, reflected, and transmitted voltage waveforms (denoted as $V_{inc}(\omega)$, $V_{refl}(\omega)$, and $V_{tran}(\omega)$) are determined first. Each of these is obtained by integrating over the corresponding E_x's underneath the center of the strip. In this study, $V_{inc}(\omega)$ and $V_{refl}(\omega)$ are observed at Z' and $V_{tran}(\omega)$ is recorded at z'' as shown in Fig. 2(a) which are away from the input and output sides of the gap (i.e., T' and T'') to avoid the irregular field behaviors near the gap. The actual spacings needed are determined as part of spatial convergence test during each calculation. For the time being, these spacings are simply denoted as L_1 and L_2, respectively. Given these, the desired S parameters can be computed from

$$S_{11}(\omega) = \frac{V_{refl}(\omega, z')}{V_{inc}(\omega, z')} \exp [j2\beta(\omega)L_1] \tag{5a}$$

and

$$S_{21}(\omega) = \frac{V_{trans}(\omega, z'')}{V_{inc}(\omega, z')} \exp [j\beta(\omega)(L_1 + L_2)]. \tag{5b}$$

These are then used to calculate the coupling and fringing capacitances C_g and C_p of the equivalent π-network model of the series gap discontinuity shown in Fig. 2(b)

$$j\omega C_g Z_0 = \frac{2S_{21}}{(1 + S_{11})^2 - S_{21}^2} \tag{6a}$$

and

$$j\omega C_p Z_0 = \frac{1 - S_{11}^2 + S_{21}^2 - 2S_{21}}{(1 + S_{11})^2 - S_{21}^2} \tag{6b}$$

where Z_0 is the characteristic impedance of the uniform line calculated as the voltage-current ratio. It is noted that since these structures are consisted of perfect dielectric and conductor, and only quasi-TEM mode propagates within the frequency range considered, they can be characterized as lossless, symmetric, and reciprocal two-port networks. As such, our data are found to obey the power conservation law of $|S_{11}|^2 + |S_{21}|^2 = 1$ and symmetry relation of $\phi_{21} = \phi_{11} + 90°$ (with $\phi_{11} \leq 0°$) [19]. Therefore, for simplicity, only the amplitude and phase of S_{21} are presented.

III. Results and Discussions

In this section, results of: 1) the effective dielectric constant of an air-filled RCTL, 2) dispersive properties of uniform SSL's and 3) scattering behaviors of series gap discontinuity in SSL's obtained by the FD-TD are discussed. For the results to be presented, the strip width (w) and groove depth (d) are allowed to be varied while the structural parameters of $h_1 = h_3 = 10$ mil, $h_2 = 5$ mil, $a = 25$ mil, $b = 50$ mil, and $\epsilon_r = 2.22$ are used in all cases except for the data shown in Fig. 5 for which $b = 25$ mil is used instead.

A. Effective Dielectric Constant of an Air-Filled RCTL

In the absence of dielectric substrate (i.e., $\epsilon_r = 1$) and mounting grooves (i.e., $d = 0$), the structure shown in Fig. 1 becomes an air-filled RCTL, which is also known as TEM cell in EMC community [20]. Given that the strip is immersed in air dielectric and single TEM mode of operation is achieved, the wave will travel at the speed of light in the RCTL and $\epsilon_{reff} = 1$ should be obtained from dc to just below the cutoff frequency of the first higher-order waveguide mode.

Gaussian pulses having f_u's of 40-, 60-, and 80-GHz are used in the FD-TD simulations. Results of ϵ_{reff} thus determined are displayed in Fig. 3. In general, results obtained for the pulse having $f_u = 60$ GHz are the best. The calculated ϵ_{reff} increases slightly from a value of 1 at dc to about 1.0015 at 80 GHz for a maximum error of 0.15%. The increasing ϵ_{reff} predicted is in accordance with the behavior of numerical dispersion inherent in the FD-TD.

For $f_u = 40$ GHz, data appear to fluctuate when frequency exceeds about 50 GHz. Since power contained in this portion of the pulse spectrum is small, its accuracy is obviously more vulnerable to the inevitable numerical noises (e.g., discretizations and round-off). On the other hand, with $f_u = 80$ GHz, the high end of pulse spectrum approaches, and actually extends beyond, the cutoff of the first higher-order mode. The propagating higher-order mode is characterized by having a phase velocity exceeds that of the speed of light. Two problems arise are: 1) stability criterion may be violated, and 2) when present, it is not accounted for in (3) (which assumes only quasi-TEM mode propagation). As a consequence, noisy data set obtained with this interrogating pulse is expected. This exercise indicates that Gaussian pulse with $f_u = 60$ GHz may be used for the determination of the properties of SSL's.

B. Dispersion in Uniform Shielded SSL

Effects of grooves on the dispersive properties of uniform SSL's are examined first. Rectangular cells, each having sidelengths of $dx = dy = a/15$ and $dz = a/7.5 = 2dx$, are found to yield results with better than 1% convergence.

In Fig. 4, ϵ_{reff} calculated for uniform SSL's with $w/b = 0.8$ and $d/b = 0$ and 0.1 are displayed. It is found that reduction in ϵ_{reff} due to grooves with $d/b = 0.1$ are less than 1% over the frequency range considered. Although not shown, results obtained for groove depth $>0.1\ b$ are essentially identical to those for $d/b = 0.1$. Fig. 5 further compares the wavelength reduction factor λ/λ_0 (or, $1/\sqrt{\epsilon_{reff}}$) for varying groove depths of $0 \leq d/b \leq 0.4$ as calculated by the FD-TD and [10] at dc for two uniform SSL's with $w/b = 0.2$ and 0.7. In this particular example, as mentioned earlier, a square housing of 25 × 25-mil is considered. In the FD-TD, static data are derived by extrapolating such frequency-dependent data as shown in Fig. 4 back to dc. As can be seen, for both SSL's, λ/λ_0 increases first (i.e., ϵ_{reff} decreases) when d/b increases

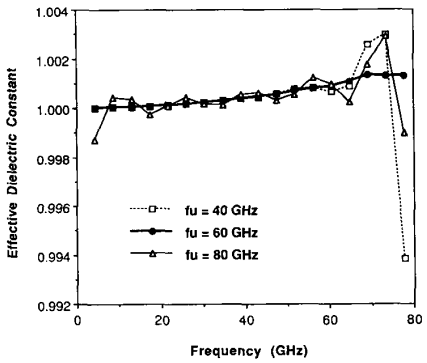

Fig. 3. Effective dielectric constant of an air-filled RCTL determined using Gaussian pulses having f_u = 40-, 60-, and 80 GHz.

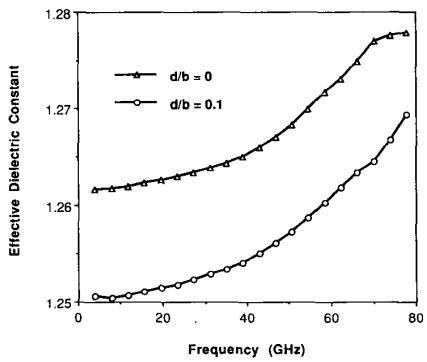

Fig. 4. Effects of sidewall mounting grooves on $\epsilon_{reff}(\omega)$ for SSL's with $w/b = 0.8$, $d/b = 0$ and 0.1. (a = 25 mil, b = 50 mil, h_2 = 5 mil).

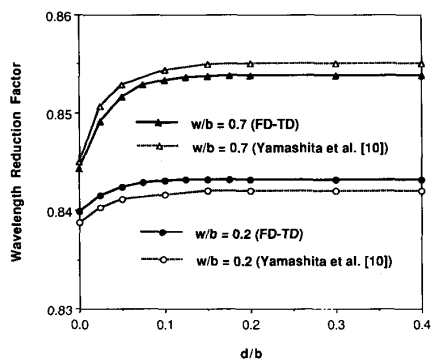

Fig. 5. Wavelength reduction factor λ/λ versus groove depth calculated for SSL's with w/b = 0.2 and 0.7 at dc. (a = 25 mil, b = 25 mil, h_2 = 5 mil).

from 0 to about 0.2 and remains constant afterwards. The maximum hike in λ/λ_0 is 0.4% when w/b = 0.2 and 1.2% when w/b = 0.7. The larger deviation in λ/λ_0 found for the SSL with wider strip is mainly due to its closer proximity and, therefore, stronger interaction with the groove. Finally, Fig. 5 shows that our data agree to within 0.12% (in λ/λ_0) of those of [10], which further confirms the accuracy of the FD-TD.

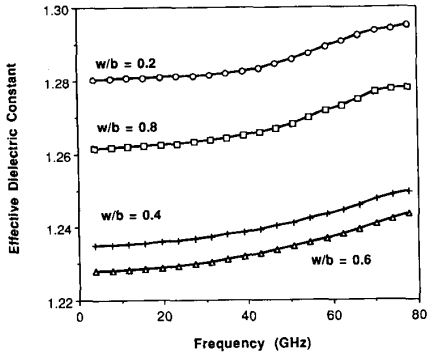

Fig. 6. Effective dielectric constant calculated for SSL's with w/b = 0.2, 0.4, 0.6 and 0.8 in the absence of grooves. (a = 25 mil, b = 50 mil, h_2 = 5 mil).

Fig. 6 summarizes ϵ_{reff} calculated for SSL's with w/b = 0.2, 0.4, 0.6, and 0.8 and d/b = 0. In general, ϵ_{reff} increases as frequency gets higher. It shows that ϵ_{reff} decreases first when w/b increases from 0.2 to 0.6 but increases again when strip width becomes $0.8b$. It is interesting to note that ϵ_{reff} increases with strip width in the case of microstrip with grounded substrate. For $w < 0.6b$, widening in the strip width apparently causes more fields to be spread into the air region such that decreasing ϵ_{reff} are observed in Fig. 6. At w/b = 0.8, the strip edge is now closer to the sidewall (at a spacing of $0.1b$ or, $0.2a$) than to the top/bottom walls. More field lines will now reach the sidewall through the substrate, an increase in ϵ_{reff} is thus expected. Similarly, with a smaller sidewall spacing of b = 25 mil, larger static ϵ_{reff}'s are observed for the two SSL's considered in Fig. 5 than those of the four SSL's shown in Fig. 6 (which are derived for b = 50 mil).

C. Scattering from Series Gap Discontinuity in Shielded SSL

In this subsection, effects of grooves are investigated first. Coupling and fringing capacitances calculated for SSL's with w/b = 0.8, g = 1 dz = $b/15$, and d/b = 0 and 0.1 are shown in Fig. 7. Since results obtained for the grooves with d/b = 0.1 (and deeper ones) are almost identical to the cases without grooves, effects of grooves may be ignored. Thus d/b is set to zero in the results to be presented next. Fig. 7 further shows that both capacitances are nearly frequency-independent. Therefore, only the extrapolated static capacitance values will be quoted for the structures to be presented later.

In Fig. 8, frequency variations of S_{21} are plotted for SSL's with w/b = 0.4 and g/dz = 1, 2, 3, 4, and 9 ($1dz$ = $a/7.5$ = $b/7.5$ = $b/15$). As expected, $|S_{21}|$ decreases with increasing gap width but increases with frequency. On the other hand, ϕ_{21} with increasing gap width but decreases with frequency. In the order of increasing gap width, the static values of C_g (10^{-3} pF) are 12.38, 6.76, 4.23, 2.76, and 0.36, and the corresponding C_p's (10^{-3}

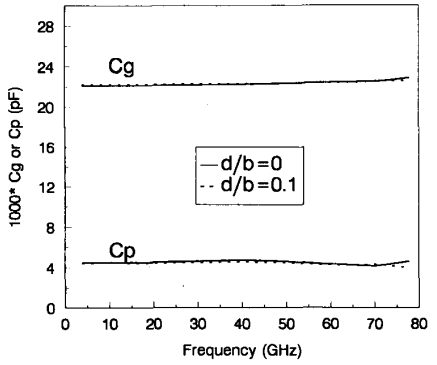

Fig. 7. Effects of sidewall mounting grooves on the coupling and fringing capacitances of SSL with $w/b = 0.8$ and $g = 1dz = b/15$. ($a = 25$ mil, $b = 50$ mil, $h_2 = 5$ mil).

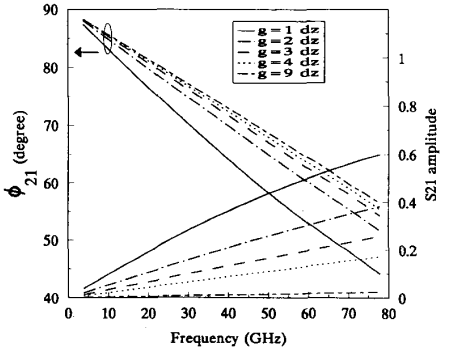

Fig. 8. Amplitude and phase of S_{21} obtained for SSL's with $w/b = 0.4$ and $g/dz = 1, 2, 3, 4$, and 9. ($a = 25$ mil, $b = 50$ mil, $h_2 = 5$ mil, $d/b = 0$, $1dz = b/15$.)

pF) are 2.51, 4.43, 5.87, 6.93, and 9.02; which show that C_g decreases while C_p increases as gap widens. For practical purposes, the gap with $g = 9dz$ may be considered to approach an open-end discontinuity.

Next, we consider the frequency dependencies of S_{21} for SSL's with $w/b = 0.2$, 0.4, 0.6, and 0.8 and $g = 2dz$. Fig. 9 depicts that $|S_{21}|$ increases and ϕ_{21} decreases as frequency increases. Similar to the behavior of ϵ_{reff} shown in Fig. 6, $|S_{21}|$ increases and ϕ_{21} decreases first when w/b increases from 0.2 to 0.6, but the trend reverses as w increases to $0.8b$. In this later case, the spacing between the edge of the strip and the sidewall is smaller than the gap width. It appears then that the approaching sidewalls may have attracted part of the energy that'd have been coupled across the gap in the cases of narrower strip. However, when the characteristic impedance is taken into account (which, over the w/b range considered here, decreases as strip width increases), both C_g and C_p are found to increase monotonically (but not linearly) with increasing strip width. In the order of increasing strip width, the static values of C_g (10^{-3} pF) are 3.80, 6.76, 9.52, and 11.78, and the corresponding C_p's (10^{-3} pF) are 2.97, 4.43, 5.95, and 7.87; which show that both capacitances increases as strip gets wider.

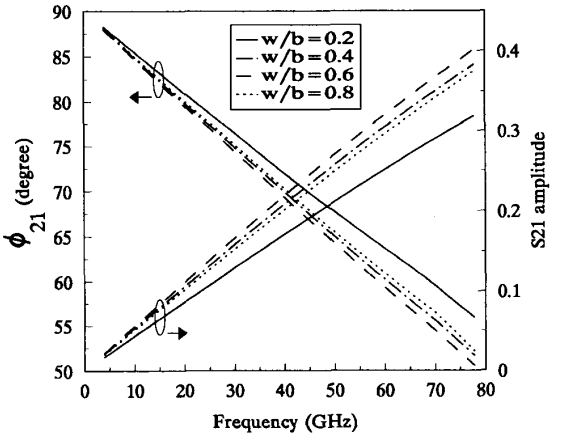

Fig. 9. Amplitude and phase of S_{21} obtained for SSL's with $w/b = 0.2$, 0.4, 0.6, and 0.8 and $g = 2dz$. ($a = 25$ mil, $b = 50$ mil, $h_2 = 5$ mil, $d/b = 0$, $1dz = b/15$.)

TABLE I
COMPARISONS OF EQUIVALENT CIRCUIT PARAMETERS OBTAINED FOR SERIES GAP DISCONTINUITIES IN SSL'S AND MICROSTRIP LINES WITH $g/dz = 1$ AND 2: (a) C_g AND (b) C_p ($a = 25$ mil, $b = 50$ mil, $h_2 = 5$ mil, $d/b = 0$, $w/d = 0.4$, $1dz = b/15$)

	$C_g(10^{-3}$ pF)		$C_p(10^{-3}$ pF)	
	$g = 1\ dz$	$g = 2\ dz$	$g = 1\ dz$	$g = 2\ dz$
SSL	12.38	6.76	2.51	4.89
Microstrip	8.92	3.71	4.43	7.88

Finally, Table I compares the static values of C_g and C_p calculated for two SSL's with $w/b = 0.4$ and $g/dz = 1$ and 2 to the corresponding cases of microstrip gap discontinuity having the same housing size and substrate thickness. It is found that for a given gap width, SSL exhibits lower fringing capacitance and higher coupling capacitance than the corresponding microstrip line. The smaller C_p observed for the SSL is apparently due to the presence of the air gap below the substrate.

IV. CONCLUSION

Dispersion and series gap discontinuity of shielded SSL's using low dielectric constant Duroid substrate ($\epsilon_r = 2.22$) are analyzed with the FD-TD. In general, presence of sidewall mounting grooves causes only a slight decrease in the ϵ_{reff} for uniform SSL's and an insignificant amount of change in the equivalent circuit parameters for the series gap discontinuity. Therefore, for practical purposes, they may be ignored.

It is found that, for a given housing, ϵ_{reff} decreases first with an increase in strip width before increasing again when strip is wider enough to interact strongly with the sidewalls. In addition, for the two housings considered, almost 10% larger ϵ_{reff}'s are observed for the housing with smaller sidewall spacings. Since small housing size is necessary for the SSL to operate in quasi-TEM mode up

to mm-wave frequencies, the above observations suggest that proximity effects should be fully considered in the circuit design process. Finally, for the gap discontinuity, stronger coupling across the gap is found as expected for wider strips and/or narrower gap width. Irregular transmission behavior is also found when strip is wide enough to interact strongly with the sidewalls.

REFERENCES

[1] T. Itoh, "Overview of quasi-planar transmission lines," *IEEE Trans. Microwave Theory Tech.*, vol. 37, pp. 275–280, Feb. 1989.

[2] R. S. Tahim, G. M. Hayashibara, and K. Chang, "Design and performance of W-band broad-band integrated circuit mixers," *IEEE Trans. Microwave Theory Tech.*, vol. MTT-31, pp. 277–283, Mar. 1983.

[3] C. I. Mobbs and J. D. Rhodes, "A generalized Chebyshev suspended substrate stripline bandpass filter," *IEEE Trans. Microwave Theory Tech.*, vol. MTT-31, pp. 397–402, May 1983.

[4] L. Q. Bui, Y. C. Shih, and T. N. Ton, "MM-wave harmonic-reject filter," *Microwave J.*, vol. 30, pp. 119–122, July 1987.

[5] R. H. Jansen, "Unified user-oriented computation of shielded, covered, and open planar microwave and millimeter-wave transmission-line characteristics," *Proc. IEE*, pt. H, vol. 3, pp. 14–22, Jan. 1979.

[6] H. Hofmann, "Dispersion of planar waveguides for millimeter-wave applications," *AEU*, vol. 31, pp. 40–44, Jan. 1977.

[7] E. Yamashita and K. Atsuki, "Analysis of microstrip-like transmission lines by nonuniform discretization of integral equations," *IEEE Trans. Microwave Theory Tech.*, vol. MTT-24, pp. 195–200, Apr. 1976.

[8] R. H. Jansen, "Hybrid mode analysis of end effects of planar microwave and millimeter-wave transmission lines," *Proc. IEE*, vol. 128, pt. H, pp. 77–86, Apr. 1981.

[9] N. H. L. Koster and R. H. Jansen, "The equivalent circuit of the asymmetric series gap in microstrip and suspended substrate lines," *IEEE Trans. Microwave Theory Tech.*, vol. MTT-30, pp. 1273–1279, Aug. 1982.

[10] E. Yamashita, B. Y. Wang, K. Atsuki, and K. R. Li, "Effects of side-wall grooves on transmission characteristics of suspended striplines," *IEEE Trans. Microwave Theory Tech.*, vol. MTT-33, pp. 1323–1328, Dec. 1985.

[11] S. B. Cohn and G. D. Osterhues, "A more accurate model of the TE_{10} type waveguide mode in suspended substrate," *IEEE Trans. Microwave Theory Tech.*, vol. MTT-30, pp. 293–294, Mar. 1982 (Also see correction, *IEEE Trans. Microwave Theory Tech.*, p. 1297, Aug. 1982).

[12] K. S. Yee, "Numerical solution of initial boundary value problems involving Maxwell's equations in isotropic media," *IEEE Trans. Antennas Propagat.*, vol. AP-14, pp. 302–307, May 1966.

[13] X. Zhang, J. Fang, K. K. Mei, and Y. Liu, "Calculations of the dispersive characteristics of microstrips by the time-domain finite difference method," *IEEE Trans. Microwave Theory Tech.*, vol. 36, pp. 263–267, Feb. 1988.

[14] X. Zhang and K. K. Mei, "Time-domain finite difference approach to the calculation of the frequency-dependent characteristics of microstrip discontinuities," *IEEE Trans. Microwave Theory Tech.*, vol. 36, pp. 1775–1787, Dec. 1988.

[15] L. K. Wu and Y. C. Chang, "Characterization of the shielding effects on the frequency-dependent effective dielectric constant of the waveguide-shielded microstrip using the finite-difference time-domain method," *IEEE Trans. Microwave Theory Tech.*, vol. 39, pp. 1688–1693, Oct. 1991.

[16] A. Taflove and M. E. Brodwin, "Numerical solution of steady-state electromagnetic scattering problems using the time-dependent Maxwell's equations," *IEEE Trans. Microwave Theory Tech.*, vol. MTT-23, pp. 623–630, Aug. 1975.

[17] D. M. Sheen, S. M. Ali, M. D. Abouzahra, and J. A. Kong, "Application of the three-dimensional finite-difference time-domain method to the analysis of planar microstrip circuits," *IEEE Trans. Microwave Theory Tech.*, vol. 38, pp. 849–857, July 1990.

[18] J. Fang and K. K. Mei, "A super-absorbing boundary algorithm for solving electromagnetic problems by time-domain finite-difference method," in *IEEE AP-S Int. Symp. Dig.*, Syracuse, NY, June 1988, pp. 472–475.

[19] V. Rizzoli and A. Lipparini, "A resonance method for the broadband characterization of general two-port microstrip discontinuities," *IEEE Trans. Microwave Theory Tech.*, vol. MTT-29, pp. 655–660, July 1981.

[20] M. L. Crawford, "Generation of standard EM fields using TEM transmission cells," *IEEE Trans. Electromagn. Compat.*, vol. EMC-16, pp. 189–195, Nov. 1974.

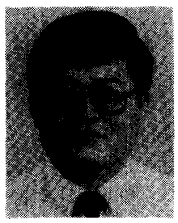

Lin-Kun Wu (S'81–M'86) was born in Hsinchu, Taiwan, Republic of China, on November 1, 1958. He graduated from Taipei Institute of Technology in 1978, and received the M.S. and Ph.D. degrees in electrical engineering from the University of Kansas, Lawrence in 1982 and 1985, respectively.

From November 1985 to December 1987, he was a Postdoctoral Research Associate at the Center for Research, Inc. of the University of Kansas, working on microwave remote sensing and computational electromagnetics. Since February 1988, he has been an Associate Professor at the Institute of Communication Engineering, National Chiao Tung University, Hsinchu, Taiwan. His current research interests involve the development of the finite-difference time-domain method and the method of moments for the characterization of microstrip and waveguide discontinuities, and for the analysis of electromagnetic scattering problems. He is also interested in radar systems and radar remote sensing.

Horng-Ming Chang was born in Taichung, Taiwan, Republic of China on September 19, 1967. He received the B.S. and M.S. degrees in communication engineering in 1989 and 1991, respectively, from National Chiao Tung University, Hsinchu, Taiwan. His M.S. thesis dealt with the analysis of shielding effects on the properties of uniform suspended substrate line and the associated series gap discontinuity.

Mr. Chang's research interests include computational electromagnetics and radar systems.